

Interpretation of *HINODE* SOT/SP asymmetric Stokes profiles observed in quiet Sun network and internetwork

B. Viticchié^{1,2}, J. Sánchez Almeida³, D. Del Moro², and F. Berrilli²

¹ ESA/ESTEC RSSD, Keplerlaan 1, 2200 AG Noordwijk, Netherlands e-mail: bartolomeo.viticchie@esa.int

² Dipartimento di Fisica, Università degli Studi di Roma “Tor Vergata”, Via della Ricerca Scientifica 1, I-00133 Roma, Italy e-mail: delmoro@roma2.infn.it, berrilli@roma2.infn.it

³ Instituto de Astrofísica de Canarias E-38205 La Laguna, Tenerife, Spain e-mail: jos@iac.es

Preprint online version: October 4, 2010

ABSTRACT

Aims. Stokes profiles emerging from the magnetized solar photosphere and observed by SOT/SP aboard the *Hinode* satellite present a variety of complex shapes. These are indicative of unresolved magnetic structures that have been overlooked in the inversion analyses performed so far. Here we present the first interpretation of the Stokes profile asymmetries measured in the Fe I 630 nm lines by SOT/SP, in both quiet Sun internetwork (IN) and network regions.

Methods. The inversion is carried out under the hypothesis of Micro-Structured Magnetized Atmosphere (MISMA), where the unresolved structure is assumed to be optically thin. We analyze a $29.52'' \times 31.70''$ subfield carefully selected to be representative of the properties of a $302'' \times 162''$ quiet Sun field-of-view at disk center.

Results. The inversion code is able to reproduce the observed asymmetries in a very satisfactory way, including the 35 % of inverted profiles presenting large asymmetries. The inversion code interprets 25 % of inverted profiles as emerging from pixels in which both positive and negative polarities coexist. These pixels are located either in frontiers between opposite polarity patches or in very quiet regions. kG field strengths are found at the base of the photosphere in both network and IN; in the case of the latter, both kG fields and hG fields are admixed. When considering the magnetic properties at the mid photosphere most kG fields are gone, and the statistics is dominated by hG fields. According to the magnetic filling factors derived from the inversion, we constrain the magnetic field of only 4.5 % of the analyzed photosphere (and this percentage reduces to 1.3 % when referred to all pixels, including those with low polarization not analyzed). The rest of the plasma is consistent with the presence of weak fields not contributing to the detected polarization signals. The average flux densities derived in the full subfield and in IN regions are higher than the ones derived from the same dataset by Milne-Eddington inversion.

Conclusions. The existence of large asymmetries in *Hinode* SOT/SP polarization profiles is uncovered. These are not negligible in quiet Sun data. The MISMA inversion code reproduces them in a satisfactory way, and provides a statistical description of the magnetized IN and network which partly differs and complements the results obtained so far. From this it follows the importance of having a complete interpretation of the line profile shapes.

Key words. Sun: surface magnetism — Sun: photosphere — Techniques: polarimetric

1. Introduction

The spectropolarimeter SOT/SP (Lites et al. 2001; Tsuneta et al. 2008) aboard the Japanese *Hinode* satellite (Kosugi et al. 2007) combines $0''.32$ angular resolution and 10^{-3} polarimetric sensitivity to perform seeing-free full Stokes measurements of the polarized light emerging from the magnetized solar photosphere. Since its launch in 2006, the SOT/SP instrument has allowed the solar community to investigate the solar surface magnetism under unprecedented stable conditions.

Hinode SOT/SP observations have been largely exploited to investigate the quiet Sun magnetism. Its global properties have been described by Orozco Suárez et al. (2007a), Lites et al. (2008), Asensio Ramos (2009), and Jin et al. (2009); while detailed analyses of its local properties, in relation with the temporal evolution due to the interaction with plasma motions, have been carried out by Centeno et al. (2007), Orozco Suárez et al. (2008), Nagata et al. (2008), Shimizu et al. (2008), Fischer et al. (2009) and Zhang et al. (2009).

The above studies have been performed exploiting inversion techniques for interpretation of the observed Stokes profiles. In most of the cases, the hypothesis of ME atmosphere has been adopted to infer the properties of the magnetic field vector in *Hinode* resolution elements. It assumes that the polarization is produced in an atmosphere where the magnetic field vector is constant. This approximation is a good compromise to interpret large data sets in reasonable times, as the ones obtained by *Hinode*. However, it is important to realize that *Hinode* angular resolution is still too low to perform spectropolarimetric observations of magnetic structures that can be regarded as uniform (e.g., Sánchez Almeida 2004; Stenflo 2009). As we emphasize in § 3.1, asymmetric Stokes profiles in *Hinode* quiet Sun observations are the rule rather than the exception, which implies the presence of unresolved structure (Sánchez Almeida et al. 1996, and references therein). The ME analyses cannot reproduce them, overlooking the

expected coexistence of several magnetic components in a single resolution element¹.

Sánchez Almeida et al. (1996) put forward arguments for describing the atmosphere where the polarization is formed as a Micro-Structured Magnetic Atmosphere (MISMA), i.e., an atmosphere in which magnetic fields have structure smaller than the photon mean-free path at the solar photosphere ($\lesssim 100$ km). It can be regarded as a limiting case of structures of all sizes (e.g. Landi Degl'Innocenti 1994a,b). The MISMA hypothesis simplifies the radiative transfer, yet it provides realistic asymmetric Stokes profiles. Under this hypothesis, the polarization from a single pixel in spectropolarimetric observations is equivalent to that produced by the average atmosphere. If one considers several components with diverse physical properties (i.e., thermodynamics, plasma motions, and magnetic fields), the resulting spectrum is not a linear combination of Stokes profiles emerging from each magnetic component. Rather, the superposition is non-linear, giving rise to asymmetries with the properties observed in the Sun (e.g., with spectral lines that produce net circular polarization). Sánchez Almeida & Lites (2000) showed how such a complex scenario can be properly adapted using a three component model MISMA, whose implementation in an inversion code (Sánchez Almeida 1997) allowed them to reproduce the full variety of profile asymmetries emerging from the quiet Sun when observed with the instrumentation available at the time. Stokes profiles in IN and network observations performed with *Hinode* exhibit very important asymmetries which encouraged us to attempt the same MISMA analysis on these data.

We present an orderly inversion of Stokes profiles observed by *Hinode* SOT/SP in IN and network regions. It is performed using the inversion code in Sánchez Almeida (1997), that has been recently employed to explain the reverse polarity patches found by *Hinode* in sunspot penumbrae (Sánchez Almeida & Ichimoto 2009). Our work represents the first analysis of quiet Sun SOT/SP data that is able to reproduce the asymmetries of the Stokes profiles. It allows us to obtain information contained in Stokes profiles that are hidden to the ME analysis. In particular, we constrain the physical properties of the unresolved magnetic structure creating the asymmetries.

The paper is structured as follows: in § 2 we briefly present the dataset and the selection of a sample subfield representative of the whole field-of-view (FOV). In § 3 the inversion hypotheses are exposed in detail, together with the adopted inversion strategy, and a few inversion examples (§ 3.1). The main results from the analysis are presented in § 4. These are then discussed in § 5. An outline of conclusions is given in § 6.

2. Dataset and subfield selection

We analyze full Stokes profiles of a $302'' \times 162''$ portion of the solar photosphere observed at disk center on 2007 March 10 between 11:37 and 14:34 UT. The spectropolarimetric measurements have been taken by the SOT/SP instrument aboard *Hinode* in the two Fe I 630 nm lines, with a wavelength sampling of $2.15 \text{ pm pixel}^{-1}$, and a spa-

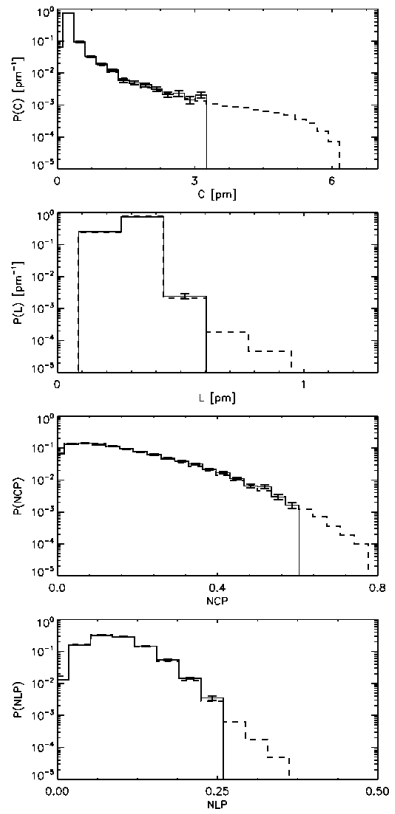


Fig. 1. Comparison between the statistical properties of the full $302'' \times 162''$ FOV (dashed line) and the statistical properties of the selected $29.52'' \times 31.70''$ subfield (solid line). From top to bottom: histogram of circular polarization (C , first plot), total linear polarization (L , second plot), net-circular polarization (NCP , third plot), and net-linear polarization (NLP , fourth plot). The error bars are defined as the square root of the number of counts in each bin.

tial sampling of $0.1476'' \text{ pixel}^{-1}$ and $0.1585'' \text{ pixel}^{-1}$ along the east-west and south-north directions, respectively. The dataset has been already analyzed by Orozco Suárez et al. (2007a), Lites et al. (2008) and Asensio Ramos (2009) to derive magnetic properties of IN and network regions.

The data reduction and calibration have been performed using the `sp_prep.pro` routine available in solar soft (Ichimoto et al. 2008). For a correct absolute wavelength calibration, a correction for the gravitational redshift of 613 m s^{-1} has been taken into account. Using the polarization signals in continuum wavelengths, we estimated a noise level of $\sigma_V \simeq 1.1 \times 10^{-3} I_c$ for Stokes V , and of $\sigma_Q \simeq \sigma_U \simeq 1.2 \times 10^{-3} I_c$ for Stokes Q and U (I_c stands for the continuum intensity).

The inversion is carried out on a $29.52'' \times 31.70''$ subfield (equivalent to 200×200 pixels) of the full FOV. MISMA inversions are time consuming, and this selection permits the in-depth analysis of a representative FOV in a reasonable timescale. The representative subfield has been selected based on two criteria. First, we consider invertible only those Stokes profiles presenting a maximum amplitude in Stokes V or Q or U above 4.5 times their noise. This check is performed in two different wavelength windows centered

¹ ME codes consider the existence of a field-free atmosphere portion in the resolution element via a stray-light filling factor (see e.g., Skumanich & Lites 1987; Orozco Suárez et al. 2007a).

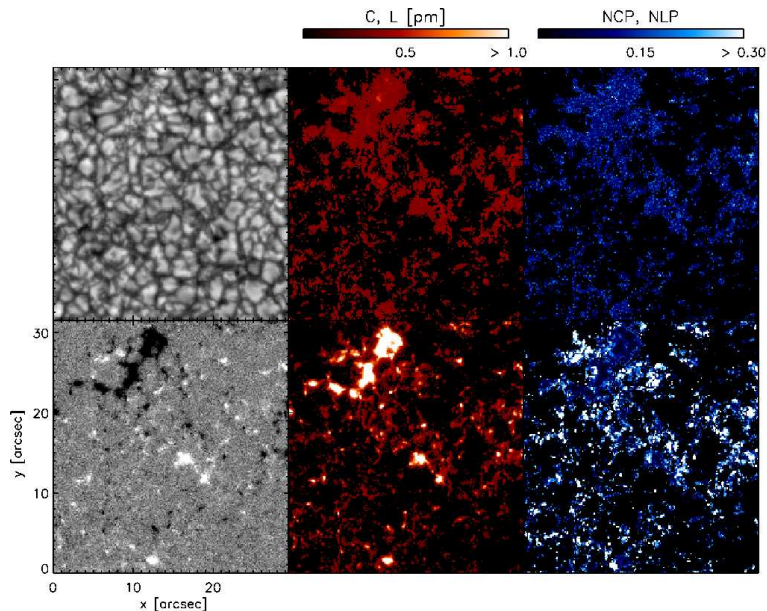


Fig. 2. Main observational properties of the representative $29.52'' \times 31.70''$ subfield selected for in-depth analysis. Continuum intensity (upper-left panel), total linear polarization (L , upper-central panel), net-linear polarization (NLP , upper-right panel), COG magnetogram saturated at ± 200 G (lower-left panel), total circular polarization (C , lower-central panel), and net-circular polarization (NCP , lower-right panel). The total polarization maps are both saturated at 1 pm, while the net-circular and net-linear polarization maps are saturated at 0.3. Black pixels in L , C , NLP , and NCP maps represent regions with signals below the threshold for inversion. The bars on top represent the color palettes adopted for the two pairs of images below them

on the two spectral lines². Second, the subfield must be a good representation of the whole set of invertible data attending to the statistical properties of the total circular polarization ($C = \int \sqrt{V(\lambda)^2 d\lambda} / I_c$), total linear polarization ($L = \int \sqrt{Q(\lambda)^2 + U(\lambda)^2 d\lambda} / I_c$), net-circular polarization ($NCP = |\Delta V| / \int |V(\lambda)| d\lambda$)³, and net-linear polarization ($NLP = (|\Delta Q| + |\Delta U|) / \int |Q(\lambda)| + |U(\lambda)| d\lambda$)⁶. The distributions employed to characterize the statistical properties of the full FOV and subfields use 30 bins to sample the full domain of each quantity. Bins with less than 16 counts in the case of the subfields, or 25 in the case of the full FOV, are discarded. In the subfield selection procedure, all possible $29.52'' \times 31.70''$ subfields in the $302'' \times 162''$ FOV are considered. The selected subfield is the one that minimizes the sum of differences between the subfield distributions and the ones defined over the $302'' \times 162''$ domain. Fig. 1 compares both the $302'' \times 162''$ statistics and the selected subfield statistics, while Fig. 2 contains the selected subfield continuum intensity represented together with the center-of-gravity magnetogram (COG; see Rees & Semel 1979), and the C , L , NCP , and NLP maps.

3. Inversion hypothesis and strategy

In order to assign physical properties to each point of the portion of photosphere under examination, we work out

² Each wavelength window is defined by two wavelengths (λ_A and λ_B) centered around the wavelength of the Stokes I minimum (λ_m). The width of the window centered on the Fe I 630.15 nm line is 86 pm, while for Fe I 630.25 nm the width is 64 pm.

³ $\Delta S = \int_{\lambda_A}^{\lambda_m} |S(\lambda)| d\lambda - \int_{\lambda_m}^{\lambda_B} |S(\lambda)| d\lambda$, where S can be Q , U , or V , and λ_A , λ_B , and λ_m are defined in footnote ².

a model atmosphere producing Stokes profiles as close as possible to the observed ones. In the technical literature, this procedure is usually referred to as *Stokes profile inversion*. We perform the inversion under the MISMA hypothesis. In a Micro-Structured Magnetized Atmosphere, magnetic fields vary over scales smaller than the photon mean-free-path at the solar photosphere (Sánchez Almeida et al. 1996; Sánchez Almeida 1997). Starting from this hypothesis, Sánchez Almeida & Lites (2000) derived by inversion eleven classes of MISMA models representative of typical profiles observed in IN and network regions at disk center.

All these models are formed by three components: one of them is field-free, while the other two are magnetized. The field-free component represents the non-magnetized plasma in which the magnetic fields are embedded, while the two magnetized components allow us to model the coexistence, in the resolution element, of different magnetic fields contributing to the formation of the observed polarization profiles. It has been shown by Sánchez Almeida et al. (1996, § 4.2) that, under the MISMA hypothesis, three is the minimum number of components with constant magnetic field required to reproduce the asymmetries of the Stokes profiles observed in the network, and three seem to suffice to reproduce all quiet Sun profiles (Sánchez Almeida & Lites 2000). Such components should be considered as a schematic representation of the average properties of the atmosphere (see Sánchez Almeida & Lites 2000, § 5). Each component of the model is characterized by the variation with height of the thermodynamical properties, plasma motions along the magnetic field lines, occupation fraction, and magnetic field strengths. These variations are forced to conserve magnetic flux and mass flows. The temperature stratification is imposed to be the same in the three optically thin components, since we expect an efficient radiative thermal ex-

change among them. Moreover, the lateral pressure balance links the properties of the components at every height; they must have the same total pressure defined as the sum of the gas pressure plus the magnetic pressure. The mechanical balance couples the magnetic field and the thermodynamics in the model atmosphere. Magnetic field inclination and azimuth are constant with height. Finally, an unpolarized stray-light contribution is considered (for a complete description of the inversion code and hypotheses, see Sánchez Almeida 1997; Sánchez Almeida & Lites 2000). The inversion of the some 400 wavelengths defining each set of Stokes profiles employs only 20 free parameters, which still are twice the number of free parameters of ME inversions (Orozco Suárez et al. 2007c).

The adopted inversion strategy is the following. Stokes I and V are inverted in those pixels presenting $|V|$ amplitude above $4.5 \times \sigma_V$ at least for one wavelength in one of the two FeI lines. If $|Q|$ or $|U|$ amplitude is above $4.5 \times \sigma_{Q,U}$, at least for one wavelength in one of the two FeI lines, a full Stokes inversion is also performed. According to these criteria about 29 % of the subfield has been inverted, with 2.3 % corresponding to full Stokes inversions. The $4.5 \times \sigma_{Q,U,V}$ thresholds have been chosen so as to be the same as that of the ME inversion analyses already performed on our dataset (Orozco Suárez et al. 2007a; Asensio Ramos 2009). Each profile has been inverted using as initial guess all the eleven classes of MISMA models of Sánchez Almeida & Lites (2000). Among the eleven inversions, we select the one having the smallest deviation between the observed and the computed profiles. Note that when only Stokes I and V are inverted, we assume the magnetic field to be longitudinal for both the magnetic components (i.e., the inclination is either zero or 180°). As we argue in Appendix A, this assumption influences the fraction of stray light inferred from the inversion, but not the magnetic field strength.

3.1. Inversion examples

In this section we present examples of inversions. They have been selected among all the 11600 inverted profiles, and they are representative of the goodness of the fit.

Fig. 3 shows three examples of pixels where the inversion code retrieves two opposite polarity fields coexisting in the resolution element. They have been picked in different regions of the subfield, i.e., around the negative network patch on the top-left corner of Fig. 2, and in IN regions. The profiles show how the two polarities can be either easily detectable, when quasi symmetric Stokes V profiles are measured, or almost hidden, when one of the two lobes of Stokes V almost vanishes. Two of the three selected cases coincide with a spatially-resolved large-scale change of polarity, i.e., the inverted pixels correspond to frontiers between positive and negative polarities in the COG magnetogram. In addition, the third example in Fig. 3 shows that mixed polarities can be found associated with polarized pixels that are not in frontiers between opposite polarities. Note that the three cases reported in Fig. 3 show no evidence of linear polarization signals above the $4.5 \times \sigma_{Q,U}$ threshold. Even below the imposed threshold, the linear polarization profiles do not present any shape that could be interpreted through an inversion procedure with reliability.

Figure 4 contains three examples of profiles observed far from network regions. They have been chosen to be char-

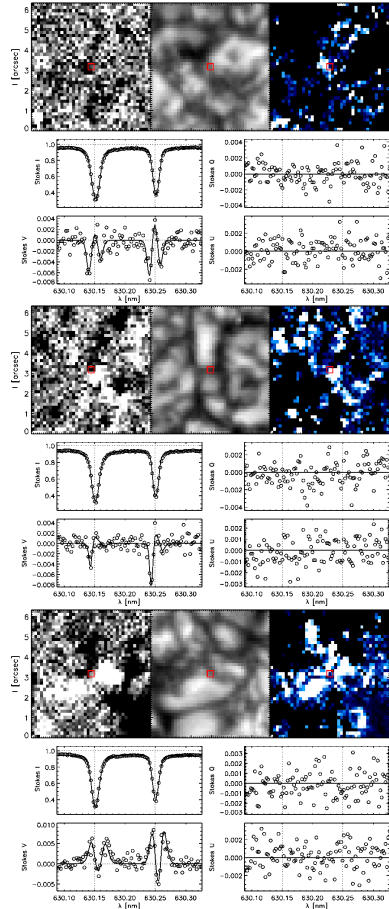


Fig. 3. Examples of MISMA inversion of *Hinode* SOT/SP Stokes profiles corresponding to mixed polarities in the resolution element. We show profiles in three different pixels representative of a weakly polarized IN region (upper panels), and frontier pixels between regions with opposite polarity in the IN (central panels) and network (lower panels). The results are organized in two sets of panels; each of these sets contains an upper row with images that put the pixel into context, and a lower row with the four Stokes profiles (as labeled). The upper row shows $l \times l$ ($l \simeq 6''$) maps of the COG magnetogram saturated at ± 50 G (left), the continuum intensity (central), and the net-circular polarization saturated at 0.3 (right). The red square indicates the position from which the profiles are taken. Lower rows: observed Stokes profiles (symbols) and best-fitting Stokes profiles (solid lines). The vertical dotted lines mark the laboratory wavelengths of the two lines.

acteristic of the typical profiles found in the IN as observed by *Hinode* SOT/SP. All Stokes V profiles present asymmetries, for which the inversion works in a really satisfactory way. The central panels of Figs. 3 and 4 correspond to adjacent pixels next to an apparent neutral line in COG magnetogram (i.e., where the magnetic field changes sign; compare their position on the magnetogram). They have been selected to show how the MISMA inversion discerns between a single polarity model (Fig. 4) and a mixed polarity model (Fig. 3). The Stokes V profile in the central panel of Fig. 3 presents a dominant negative blue lobe which indicates the presence of negative fields. Beside this, a small negative red lobe is also detected by the inversion. The

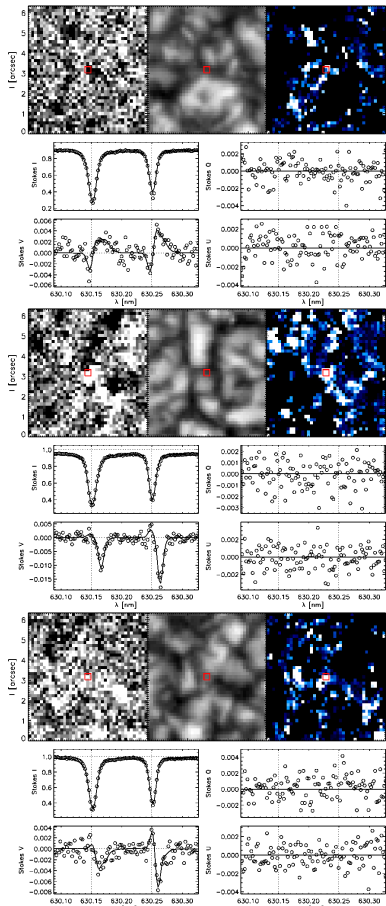


Fig. 4. Examples of MISMA inversion of *Hinode* SOT/SP Stokes profiles corresponding to a single polarity in the resolution element. For details on the layout of the figure, see the caption of Fig. 3.

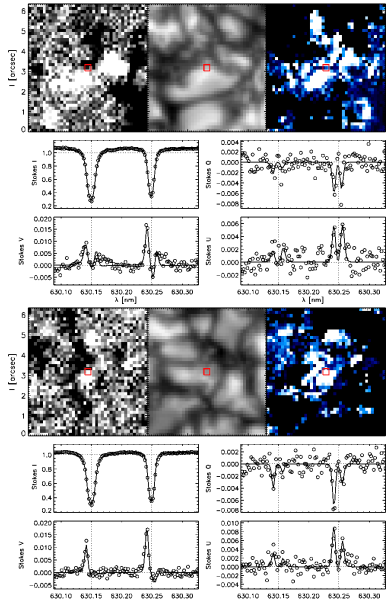


Fig. 5. Examples of full Stokes MISMA inversion of *Hinode* SOT/SP Stokes profiles. For details on the layout of the figure, see the caption of Fig. 3.

latter denotes the presence of positive fields. The MISMA code correctly interprets such a profile as emerging from a pixel in which opposite polarities coexist. Such an interpretation is consistent with the COG map, showing how the pixel from which the profile is taken lies in the frontier between positive and negative field patches. The central panel of Fig. 4 shows the Stokes V profile of a pixel next to the previous one in the direction of the positive polarity concentration. It is very different from its neighbor – the profile in Fig. 4 is dominated by a negative red lobe and presents a small positive blue lobe. The MISMA code interprets such a profile as emerging from a pixel in which only positive fields are present. In this case the inversion is also consistent with the COG magnetogram, which shows the pixel lying on a positive polarity patch.

Figure 5 presents two examples of full Stokes inversion, i.e., inversions including Q and U . Such examples illustrate the linear polarization signals we considered to be invertible. The upper panel of Fig. 5 shows the inversion of a pixel very close to the example in the upper panel of Fig. 3. In this case the linear polarization signal is strong enough to be analyzed and the MISMA code succeeds in the inversion. It is important to notice that in such a pixel, similarly to what found in the upper panel of Fig. 3, polarization profiles are still interpreted by the code as emerging from a mixed polarity pixel. In the lower panel of Fig. 5 a full inversion of an IN pixel is represented. In this case, even if the pixel is almost on the frontier between opposite polarity regions, a single polarity is measured. In the two cases the magnetic field strengths at the base of the photosphere are in the kG regime.

The examples discussed here illustrate not only the goodness of the fits but also the soundness of the MISMA interpretation of *Hinode* SOT/SP measurements. Such measurements are often characterized by important asymmetries in Stokes V profiles; Figs. 3 and 4 show three examples of Stokes V profiles whose $NCP \geq 0.3$. From the maps in Fig. 2, we notice that such values for the NCP are very common in the selected $29.52'' \times 31.70''$ subfield and, by extrapolation, they should be very common in the full FOV as well. The common presence of large asymmetries demands a refined inversion method to interpret quiet Sun SOT/SP profiles, such as the MISMA inversion we are employing. Detail on the percentage of asymmetric profiles are reported in § 4.

4. Results

The inversion code succeeded in the inversion of 11600 profiles which represent 29% of the selected subfield. The total time needed to perform such an analysis is about two days when the inversion analysis is split into eight IDL jobs running in parallel⁴. Among the 11600 inverted profiles, 925 ($\simeq 8\%$ of the total number) show invertible linear polarization signals. These profiles have been found mainly in correspondence with patches of strong polarization (see the upper panel in Fig. 5). Here we present the results obtained from the inversion of Stokes I and V profiles alone. Full Stokes inversions using modified MISMA models hav-

⁴ The inversion of each pixel is independent so the analysis of the invertible domain can be distributed over different CPUs; the jobs run on two Xeon E5410 Quad-core processors with 8 GB of shared ram.

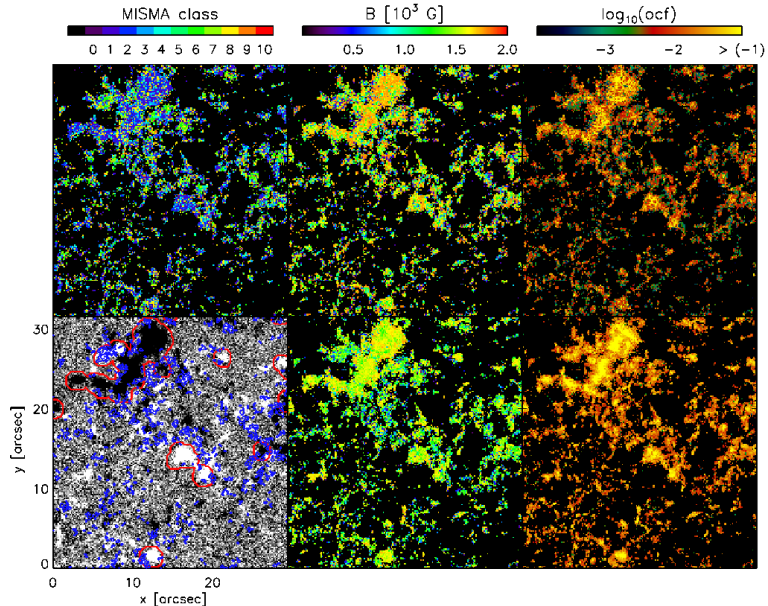


Fig. 6. Results of the inversion at the constant reference height, corresponding to the base of the photosphere. The different panels contain: classes of initial model MISMAs used in the inversion (upper-left panel), field strength for the minor component (upper-central panel), occupation fraction for the minor component (upper-right panel), COG magnetogram saturated at ± 50 G (lower-left panel), field strength for the major component (lower-central panel), occupation fraction of the major component (lower-right panel). The contours on the COG magnetogram represent the network regions as identified by our automatic procedure (red), and the pixels with mixed polarities in the resolution element (blue). Black pixels in the MISMA class, field strength, and occupation fraction maps correspond to regions that are not inverted (see Fig. 2). The bars on top represent the color palettes adopted for the MISMA initial models (on the left), and for the two pairs of images of field strength (on the center) and occupation fraction (on the right)

ing inclination and azimuth as free parameters have been performed with success (e.g., Fig. 5), but they are less representative from a statistical point of view, and they provide similar results. In fact, magnetic field strengths from few hG to kG fields are measured in fully inverted pixels, with a slightly higher probability for kG fields. We focus our analysis on the statistical properties of the magnetic field strength and occupation fraction at the photosphere as retrieved by the inversion code (the occupation fraction is just the volume filling factor). Assuming the model atmospheres to be in lateral pressure balance, each value of total pressure defines the same geometrical height in all model MISMAs. We decided to take as reference height in the atmosphere the one corresponding to the base of the photosphere in typical 1D quiet Sun model atmospheres (e.g., Maltby et al. 1986). The photospheric lower boundary in such models is defined as the height where the continuum optical depth at 500 nm equals one, which corresponds to a pressure of about 1.3×10^5 dyn cm $^{-2}$. Unless otherwise is mentioned explicitly, all the parameters discussed hereafter refer to this reference height or, equivalently, to this reference total pressure.

Fig. 6 shows six maps summarizing the inversion at the reference height, together with the COG magnetogram, used here to show the context. The red contours on the COG magnetogram separate network and IN regions in the selected subfield. Network patches have been identified using an algorithm which takes into account two properties of the IN and network regions. First, the IN covers most of the solar photosphere at any time (more than 90 % for Harvey-Angle 1993, which is the figure we use in the cal-

culations). Second, network patches are magnetic concentrations showing a spatial coherence. The network must be identified not just as a strongly polarized region; it is expected to be also spatially extended. The procedure to define the network works as follows: (1) it automatically finds the threshold on the total polarization that makes the patches of large signal to cover a few percent of the FOV ($\simeq 4\%$). These signals are tentatively identified as cores of network elements. (2) It checks the spatial extension of the network patch candidates so as to exclude connected structures composed by less than ten pixels. Once the network patches have been identified, the procedure dilates them using a 10×10 pixel square kernel. The network patches thus selected cover 11 % of the subfield.

At the location of the network patches the map showing the initial guess models for the inversion of each pixel reveals a significant degree of local coherence (Fig. 6, top left panel). On the contrary, the initial model MISMA fluctuates in the IN on scales smaller than 1''. Considering network and IN altogether, the percentages of different types of best initial guess models are class 0 $\simeq 5\%$, class 1 $\simeq 18\%$, class 2 $\simeq 16\%$, class 3 $\simeq 10\%$, class 4 $\simeq 11\%$, class 5 $\simeq 0\%$, class 6 $\simeq 7\%$, class 7 $\simeq 12\%$, class 8 $\simeq 14\%$, class 9 $\simeq 5\%$, and class 10 $\simeq 0\%$ (see Sánchez Almeida & Lites 2000 for a detailed description of the classes). The initial model MISMAs can be used as a proxy for the kind of asymmetries present in *Hinode* spectra. We find that 35 % of the inverted profiles belong to classes 4, 6, 7, 9. These are the classes where Stokes V presents large asymmetries, similar to those shown in Figs. 3 and 4.

The central panels of Fig. 6 show the magnetic field strengths for the two magnetized components of the model MISMAs. The results have been organized so that the major and the minor components are considered separately⁵. On the one hand, the major component presents occupation fractions (equivalent to volume filling factors) going from $\sim 10^{-2}$ up to $\gtrsim 10^{-1}$, and magnetic field strengths between 0 G and 1.8 kG. On the other hand, the minor component presents filling factor almost always $\lesssim 10^{-2}$ and field strengths $\gtrsim 1$ kG. Only in the network patches the minor component presents values for the filling factor comparable with the values of the major component.

The statistical properties of the field strength for both the major and minor components are reported in Fig. 7. It gives the fraction of analyzed photosphere covered by a given field strength $P_Z(B)$, i.e., except for a scaling factor, it gives the sum of all occupation fractions for each magnetic field strength B . The histograms have been defined by sampling the interval 0 – 2 kG with 20 bins of 100 G. They show the probability of finding a given field strength in our quiet Sun inversion. The distribution corresponding to the whole subfield presents a maximum at $\simeq 1.6$ kG, and then an extended tail for smaller field strengths. The statistics for the IN (Fig. 7, top, thick solid line) also shows kG fields, with a secondary maximum at the equipartition value of $\simeq 5$ hG. Note the reduction of the kG peak with respect to the full subfield distribution (Fig. 7, top, thin solid line). It is clear that the hG fields are almost completely in the IN, while the network is dominated by kG fields with little contribution for fields in the hG regime. On the other hand, the statistics of the minor component is completely dominated by strong kG fields with a maximum just at 1.8 kG and almost null hG contribution; this is valid for the whole subfield, IN, and network.

The magnetic field strength distribution in Fig. 8 is calculated for a height in the atmosphere of approximately 150 km, i.e., a height representative of the formation region of the core of the FeI lines. Similarly to what is done for the definition of the reference height of the photosphere, the heights are selected as those having a total pressure of 4×10^4 dyn cm⁻² (approximatively at 150 km in the pressure stratification of the mean photosphere; e.g., Maltby et al. 1986). The main difference between the two statistics in Figs. 7 and 8 is the large reduction of kG fields at 150 km. The magnetic structures are treated as thin flux-tubes by the inversion code, therefore, the magnetic field lines must fan out with height to maintain the mechanical equilibrium, which implies a drop in field strength, and an expansion of the magnetic structures (e.g., Spruit 1981). The two factors conspire to produce the observed increase of hG fields with height (cf. Fig. 7 and Fig. 8). For example, the volume occupied by magnetic fields smaller than 1 kG at 150 km is some 8 times larger than their volume at the base of the photosphere.

A very interesting result, unique to MISMA inversions, is the detection of a large number of mixed polarity pixels (three examples are reported in Fig. 3). These are identified by the blue contours on the COG magnetogram of Fig. 6. Pixels presenting mixed polarities are very common in IN, namely about 25 % of the total number of inverted profiles.

⁵ In each pixel, the major and the minor components are the magnetized components having the largest and the smallest mass, respectively.

On the contrary, network patches tend to be interpreted by the code as unipolar regions. We note that mixed polarities show up almost always either in the frontiers between strong signals of opposite polarity, or in low polarization regions, close to the $4.5 \times \sigma_V$ level. We also note the presence of mixed polarities surrounding the large negative polarity network patch in the selected subfield (see the upper left corner in the COG magnetogram in Fig. 6). They are always found where positive small concentrations are close to the network patch. Fig. 7 also includes the statistical properties of the mixed polarity pixels separately. Contrarily to the other statistics described above, the distribution for mixed polarity pixels is not dominated by kG fields: hG and kG fields are found almost with the same occupation fraction in both IN and network regions, and for both minor and major components. The distribution presents an absolute maximum at about 1.6 kG and a secondary one at about 500 G.

The fraction of analyzed photosphere occupied by magnetic fields α can be computed as the integral of the distributions in Fig. 7, i.e.,

$$\alpha = \int_0^\infty P_Z(B) dB. \quad (1)$$

Considering the full subfield, the value of α for the major and the minor components is 3.1 % and 1.4 %, respectively. In other words, 95.5 % of the analyzed photosphere is field free or, more precisely, it has field strengths much smaller than the ones inferred from inversion, so that the inversion code cannot distinguish them from zero. Other fractions corresponding to the various components in the FOV are listed in Table 1. The first moment of the magnetic field strength distributions also provides an estimate of the unsigned flux density $\langle B \rangle$ (see, e.g., Domínguez Cerdeña et al. 2006b),

$$\langle B \rangle = \int_0^\infty B P_Z(B) dB, \quad (2)$$

and of the average field strength,

$$\overline{B} = \langle B \rangle / \alpha. \quad (3)$$

The values of $\langle B \rangle$ and \overline{B} for the various components in the FOV are listed in Table 1. As the table shows, $\langle B \rangle = 66$ G considering network and IN all together. This flux density is so large partly because it reflects the fraction of the $29.52'' \times 31.70''$ subfield having the largest polarization signals. Such fraction f is about 0.29, therefore, if one considers the full subfield, the fraction of photosphere occupied by the magnetic fields inferred from our inversion is αf , and the unsigned flux density $\langle B \rangle f$. The values of the filling factor and unsigned flux densities corresponding to this other normalization are also included in Table 1 within parentheses. Then the unsigned flux density decreases to about 19 G. This still large value is put into context in § 5, but it is important to realize that it implicitly assumes the $(1 - f)$ non-inverted subfield to have no magnetic fields.

We have also tried a crude separation between granules and intergranules. A simple thresholding criterion was used, so that pixels brighter than the mean intensity are granules, and vice-versa. We find that 75 % of the magnetized plasma is in intergranules, and this fraction increases with increasing field strength – 85 % of the plasma having

$B > 1.5$ kG is in intergranules. These figures are meant to be rough estimates since our simple criterion is insufficient for an accurate separation between granules and intergranules.

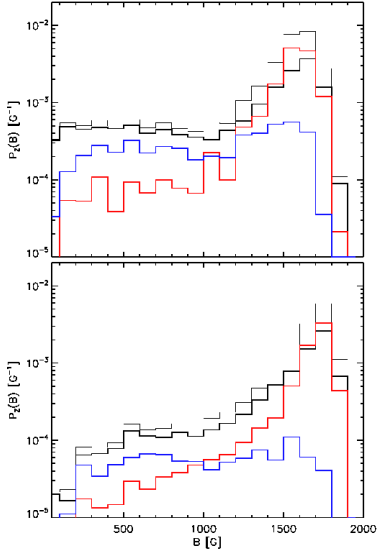


Fig. 7. Fraction of analyzed photosphere covered by a given strength. Field strength distributions for the major component (upper panel): IN (black thick line), network (red line), mixed polarity regions (blue line), and the full $29.52'' \times 31.70''$ subfield (black thin line). Field strength distributions for the minor component (lower panel).

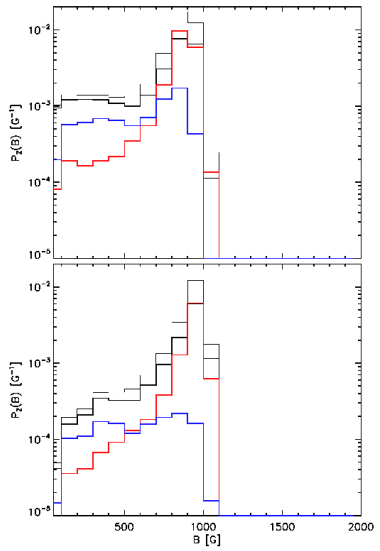


Fig. 8. Fraction of analyzed photosphere covered by a given strength at 150 km height in MISMA models. For details on the layout of the figure, see the caption of Fig. 7.

5. Discussion

The ubiquity of Stokes profiles with asymmetries implies that even *Hinode* SOT/SP resolution is insufficient to

resolve the structure of the quiet Sun magnetic fields (see Sánchez Almeida et al. 1996). This unresolved structure has been neglected in the analyses carried out so far, and we present the first attempt to account for it when interpreting *Hinode* spectra. We employ the MISMA inversion code by Sánchez Almeida (1997), which produces very good fits. The MISMA description is able to reproduce the whole range of profile shapes observed by *Hinode* SOT/SP in the quiet Sun, which are often extremely asymmetric. This was known for Advanced Stokes Polarimeter (ASP) spectra (Sánchez Almeida & Lites 2000), but *Hinode* SOT/SP has three times the spatial resolution of ASP (i.e., $0.3''$ against $1''$).

The percentages of MISMA classes used as initial guess are different from the ones reported in Sánchez Almeida & Lites (2000). This can be due either to the inversion strategy (e.g., the imposed threshold to select invertible data) or to a general modification of Stokes profile shapes due to the higher spatial resolution.

As pointed out in Sánchez Almeida & Lites (2000), the major component is the dominant source of polarization of the model since it contains the largest mass. For this reason, the statistics of the major component will be considered as the reference statistics derived from our analysis. The field strength distribution for the major component shows an important difference with respect to the results in Sánchez Almeida & Lites (2000); in fact, our analysis is able to reveal much more hG fields than the analysis of the ASP data. These are almost completely in the IN, and a large part of them are found in mixed polarity pixels. Moreover, the statistics on the latter shows that hG and kG fields are measured with the same probability. The IN kG magnetic fields are more important in our inversion than the inversions carried out by Orozco Suárez et al. (2007a) and Asensio Ramos (2009). Part of this difference is certainly due to their use of ME atmospheres, unable to reproduce the important line asymmetries characteristic of the quiet Sun Stokes profiles. Such difficulty may be secondary when dealing with slightly asymmetrical profiles, but the field strengths are inferred from the Stokes V shapes, and any field strength extracted by fitting anti-symmetric ME profiles to profiles like those in Figs. 3 and 4 is open to question. Another part of the difference can come from the large drop of magnetic field strength with height in the atmosphere. As discussed in Domínguez Cerdeña et al. (2006b) and in § 4, a reduction of the magnetic pressure is required to maintain the mechanical balance between the magnetic structures and the field free atmosphere when the gas pressure decreases exponentially with height. Such a decrease in field strength is intrinsic to the MISMA models, which force their components to be in horizontal and vertical mechanical equilibrium. Orozco Suárez et al. (2007b) showed that the ME inversion of Fe I 630 nm gives us information on the solar atmosphere at the height of formation of the lines, which is higher than the reference height adopted in this work. When the magnetic field strength statistics is calculated at a height of 150 km, then kG fields are almost absent (Fig. 8), which partly reconciles our results with those inferred from ME inversions. However, the shape of our distribution still differs from the one reported in Orozco Suárez et al. (2007a) in which the most probable field strength is $\simeq 100$ G.

Three additional comments regarding the field strength distribution are in order. First, kG fields are needed to

Table 1. Summary of magnetic properties at the base of the photosphere derived from the MISMA inversion

Portion of photosphere	Field Strength B [G]		Flux Density $\langle B \rangle$ [G]			Filling Factor α		
	major	minor	major	minor	both	major	minor	both
internetwork (IN)	1258	1521	20 (5.8)	12 (3.5)	32 (9.3)	1.6 (0.5)	0.7 (0.2)	2.3 (0.7)
mixed polarity regions	1036	1041	5 (1.6)	1 (0.3)	6 (1.9)	0.5 (0.1)	0.1 (0.0)	0.6 (0.1)
network	1513	1644	23 (6.7)	11 (3.2)	34 (9.9)	1.5 (0.4)	0.7 (0.2)	2.2 (0.6)
full subfield	1380	1578	43 (12.5)	23 (6.7)	66 (19.2)	3.1 (0.9)	1.4 (0.4)	4.5 (1.3)

Note 1. The four rows are defined from the four distributions in Fig. 7, which are normalized to the analyzed portion of photosphere, i.e., 29% of the $29.52'' \times 31.70''$ subfield. The values normalized to the whole subfield area are reported within parentheses.

explain the presence of G-band bright points in the quiet Sun intergranular lanes (e.g., Sánchez Almeida et al. 2004; de Wijn et al. 2005; Bovelet & Wiehr 2008; Sánchez Almeida et al. 2010) and, therefore, it is a sign of consistency that they show up in spectro-polarimetric observations. The occupation fraction of kG fields inferred from the inversion is of the order of a few percent, which is in good agreement with the 0.5 – 2 % G-band bright point surface coverage recently measured (Sánchez Almeida et al. 2004; Bovelet & Wiehr 2008; Sánchez Almeida et al. 2010). Moreover, the large polarization signals that we select for inversion appear preferentially in the intergranular lanes (Domínguez Cerdeña et al. 2003a; Lites et al. 2008) where the BPs are known to reside. Second, our results do not exclude the presence of weak fields (i.e., fields producing weak polarization signals in the FeI visible lines). Our inversion retrieves the field strength of only 4.5 % of the photospheric plasma (see § 4). The field strength of the rest remains unconstrained. This part is almost certainly magnetic, but with properties that remain elusive to our observation because of its complex magnetic topology that cancels Zeeman signals, because of the low field strengths, or both. Sánchez Almeida et al. (2003) and Domínguez Cerdeña et al. (2006a) show how part of these hidden fields can be revealed through MISMA inversion by analyzing FeI infra-red lines. Even weaker fields can be inferred and diagnosed via Hanle effect (e.g., Faurobert-Scholl 1994; Bommier et al. 2005). In order to avoid overlooking the weak field component, the quiet Sun regions need to be analyzed using measurements in both visible and infra-red spectral ranges, and produced by both Zeeman and Hanle effects. How to consistently combine these measurements remains an open issue, but such combination is certainly the way to go (see the first attempt by Domínguez Cerdeña et al. 2006b). The third comment on the field strength distribution refers to discarding biases that may artificially produce kG fields. Bellot Rubio & Collados (2003) show how large noise in the Stokes V profiles of the FeI 630 nm lines may fake kG fields. However, this effect is insignificant above a signal-to-noise ratio threshold that our typical spectra exceed. Moreover, in addition to kG, noise also produces false weak dG, which we do not see. Another potential source of false kG fields could be (polarized) stray-light from the network to the IN. Although we cannot discard some influence close to the network patches, stray-light cannot account for the bulk of the kG fields in the IN. Stray-light is at most 10% as measured for the broadband filter imager aboard *Hinode* (Wedemeyer-Böhm 2008). It could account for 10% of the network magnetic flux artificially appearing in the IN, but this represents only a

few G, thus unable to explain the some 30 G inferred for the IN (see Table 1).

The mixed polarity regions revealed by the MISMA analysis are about 25 % of the total number of inverted profiles, similar to the percentage reported in Sánchez Almeida & Lites (2000) for ASP data (see also Socas-Navarro & Sánchez Almeida 2002). Note that the percentage of mixed polarities has not changed despite the increase of angular resolution (from $1''$ to $0.3''$), and despite the fact that the polarization signals analyzed here are generally larger (we use a noise threshold 1.5 times larger than the one used on ASP spectra). The really significant difference between the two datasets is the fraction of solar surface covered by polarization signals; Sánchez Almeida & Lites (2000) invert only 15 % of the surface, whereas *Hinode* spectra allow us to almost double this fraction. The increase of angular resolution has certainly resolved some of the mixed polarities detected at ASP angular resolution, however, at the same time, the newly revealed Stokes V profiles uncover mixed polarities at even finer spatial scales. This observation is consistent with the numerical models of solar magneto-convection and/or turbulent dynamos (e.g., Cattaneo 1999; Vögler & Schüssler 2007). They predict an intricate pattern of highly intermittent fields varying over very small spatial scales down to the diffusion length-scales.

The average flux density we infer from the inverted profiles is of the order of 19 G when the area of the full subfield is considered for normalization (see Table 1). This value is almost twice as large as the one inferred by Sánchez Almeida & Lites (2000, $1''$ resolution), and it is also significantly larger than the ones obtained from ME inversions of quiet Sun *Hinode* spectra by Orozco Suárez et al. (2007a, ~ 9.5 G for the full FOV), and using the magnetograph equation by Lites et al. (2008, 11 G). However, our estimate is comparable with other *Hinode* based estimates of the unsigned flux of the quiet Sun (e.g., Jin et al. 2009 get 28 G). Such a difference could be explained taking into account that ME inversions are blind to sub-pixel magnetic structuring. Note that the average flux density from the major component (i.e., the dominant source of polarization) is in good agreement with Orozco Suárez et al. (2007a) and Lites et al. (2008) – we get 12.5 G, see Table 1. The small excess with respect to their results is compatible with the 1.6 G flux contribution from mixed polarities (see Table 1). The bulk of the difference seems to reside in the 6.7 G provided by the minor component. Its contribution to the flux density is more important than the modification it produces on the polarization signals (even though it is needed to reproduce the line asymmetries).

6. Conclusions

We present the first inversion of *Hinode* SOT/SP Stokes profiles that accounts for the asymmetries of the profiles in the quiet Sun. The analysis is carried out under the MISMA hypotheses which allows to reproduce the different profile shapes observed in the quiet Sun. We follow the approach already successfully exploited to describe the asymmetries observed with 1'' angular resolution (Sánchez Almeida & Lites 2000).

The main results are as follows:

1. We inverted 11600 sets of Stokes I and V profiles representative of the quiet Sun internetwork (IN) and network at disk center. The inversion code is able to reproduce, in a satisfactory way, the whole variety of asymmetries revealed by *Hinode* SOT/SP.
2. The MISMA code is also able to reproduce linear polarization measurements when full Stokes inversions are performed. Here we report a few examples.
3. The existence of asymmetries is certainly not negligible. Some 35 % of the analyzed profiles present large asymmetries, according to the rough classification used in Sánchez Almeida & Lites (2000).
4. 25% of the analyzed profiles present asymmetries that are interpreted by the MISMA code as due to mixed polarities in the resolution element. These pixels are found to be located either in transition regions between patches of opposite polarity, or in pixels presenting weak polarization signals.
5. The magnetic plasma whose properties the inversion code constrains represents only 4.5 % of the photospheric plasma. The rest remains unconstrained by our analysis.
6. The statistics of the detected magnetic field strength at the formation height of the continuum is dominated by strong kG fields, both in the network and the IN. The later, however, presents an extended tail over the whole hG domain.
7. At the height of 150 km (representative of the formation heights of the Fe I visible lines) very little kG fields are measured. This result narrows down the gap between our field strength distribution and those inferred from ME inversions by Orozco Suárez et al. (2007a) and Asensio Ramos (2009), and it follows directly from the decrease of the field strength in response to the decrease of the gas pressure with height in the photosphere.
8. The average flux density derived from the inverted pixels is 66 G. If one considers the full analyzed subfield, it becomes 19 G. The same figures for the IN become 32 G and 9.3 G, respectively. These values are significantly larger than the ones obtained from ME inversions of quiet Sun *Hinode* spectra by Orozco Suárez et al. (2007a, ~ 9.5 G for the full FOV), and using the magnetograph equation by Lites et al. (2008, 11 G). However, our estimate is comparable with other *Hinode* based estimates of the unsigned flux of the quiet Sun (e.g., Jin et al. 2009 get 28 G).

As a general concluding remark, the analysis here presented reveals the importance of a complete interpretation of the shape of Stokes V profiles through refined inversion codes. This work should be considered as the first step in the interpretation of *Hinode* SOT/SP profile shapes. Because of the wealth of information contained in the asym-

metries, such a topic deserves attention from the solar community. Different inversion codes and hypotheses can be adopted to interpret such asymmetries, and they will probably be able to reproduce the line shapes as well (e.g., a systematic variation of magnetic field and velocity along the LOS; Ruiz Cobo & del Toro Iniesta 1992). The uniqueness of the interpretation cannot be assessed unless different alternatives agree.

Acknowledgements. *Hinode* is a Japanese mission developed and launched by ISAS/JAXA, with NAOJ as domestic partner and NASA and STFC (UK) as international partners. It is operated by these agencies in co-operation with ESA and NSC (Norway). JSA acknowledges the support provided by the Spanish Ministry of Science and Technology through project AYA2007-66502, as well as by the EC SOLAIRE Network (MTRN-CT-2006-035484). This work was partially supported by ASI grant n.I/015/07/0ESS.

References

- Asensio Ramos, A. 2009, ApJ, 701, 1032
 Bellot Rubio, L. R. & Collados, M. 2003, A&A, 406, 357
 Bommier, V., Derouich, M., Landi Degl'Innocenti, E., Molodij, G., & Sahal-Bréchot, S. 2005, A&A, 432, 295
 Bovelet, B. & Wiehr, E. 2008, A&A, 488, 1101
 Cattaneo, F. 1999, ApJ, 515, L39
 Centeno, R., Socas-Navarro, H., Lites, B., et al. 2007, ApJ, 666, L137
 de Wijn, A. G., Rutten, R. J., Haverkamp, E. M. W. P., & Süttlerlin, P. 2005, A&A, 441, 1183
 Domínguez Cerdeña, I., Kneer, F., & Item on the spacial distribution of kG as related to BPs. Have you tried to whether kG tend to coincide with dark structures? Sánchez Almeida, J. 2003, ApJ, 582, L55
 Domínguez Cerdeña, I., Sánchez Almeida, J., & Kneer, F. 2006a, ApJ, 646, 1421
 Domínguez Cerdeña, I., Sánchez Almeida, J., & Kneer, F. 2006b, ApJ, 636, 496
 Faurobert-Scholl, M. 1994, A&A, 285, 655
 Fischer, C. E., de Wijn, A. G., Centeno, R., Lites, B. W., & Keller, C. U. 2009, A&A, 504, 583
 Harvey-Angle, K. L. 1993, PhD thesis, , Utrecht University, The Netherlands, (1993)
 Ichimoto, K., Lites, B., & Elmore, a. o. 2008, Sol. Phys., 249, 233
 Jin, C., Wang, J., & Zhao, M. 2009, ApJ, 690, 279
 Kosugi, T., Matsuzaki, K., Sakao, T., et al. 2007, Sol. Phys., 243, 3
 Landi Degl'Innocenti, E. 1994a, in Solar Surface Magnetism, ed. R. J. Rutten & C. J. Schrijver, 29–+
 Landi Degl'Innocenti, E. 1994b, in Solar Surface Magnetism, ed. R. J. Rutten & C. J. Schrijver, 29–+
 Lites, B. W., Elmore, D. F., & Streander, K. V. 2001, in Astronomical Society of the Pacific Conference Series, Vol. 236, Advanced Solar Polarimetry – Theory, Observation, and Instrumentation, ed. M. Sigwarth, 33
 Lites, B. W., Kubo, M., Socas-Navarro, et al. 2008, ApJ, 672, 1237
 Maltby, P., Avrett, E. H., Carlsson, M., et al. 1986, ApJ, 306, 284
 Nagata, S., Tsuneta, S., Suematsu, Y., et al. 2008, ApJ, 677, L145
 Orozco Suárez, D., Bellot Rubio, L. R., del Toro Iniesta, et al. 2007a, ApJ, 670, L61
 Orozco Suárez, D., Bellot Rubio, L. R., & del Toro Iniesta, J. C. 2007b, ApJ, 662, L31
 Orozco Suárez, D., Bellot Rubio, L. R., Del Toro Iniesta, J. C., et al. 2007c, PASJ, 59, 837
 Orozco Suárez, D., Bellot Rubio, L. R., del Toro Iniesta, J. C., & Tsuneta, S. 2008, A&A, 481, L33
 Rees, D. E. & Semel, M. D. 1979, A&A, 74, 1
 Ruiz Cobo, B., & del Toro Iniesta, J. C. 1992, ApJ, 398, 375
 Sánchez Almeida, J. 1997, ApJ, 491, 993
 Sánchez Almeida, J., Landi Degl'Innocenti, E., Martínez Pillet, V., & Lites, B. W. 1996, ApJ, 466, 537
 Sánchez Almeida, J. & Trujillo Bueno, J. 1999, ApJ, 526, 1013
 Sánchez Almeida, J. & Lites, B. W. 2000, ApJ, 532, 1215
 Sánchez Almeida, J., Domínguez Cerdeña, I., & Kneer, F. 2003, ApJ, 597, L177
 Sánchez Almeida, J., Márquez, I., Bonet, J. A., Domínguez Cerdeña, I., & Muller, R. 2004, ApJ, 609, L91

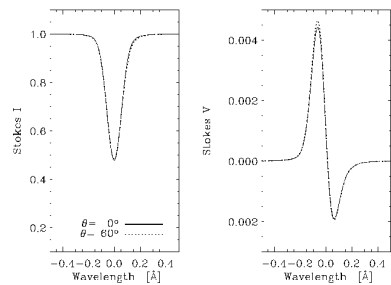


Fig. A.1. Two sets of synthetic Stokes I and V profiles of Fe I 630.25 nm obtained with different magnetic field inclinations θ but the same product $(1 - f_{sl}) \cos \theta$, with f_{sl} the fraction of stray-light. The solid and the dotted lines correspond to $\theta = 0^\circ$ and 60° , respectively. The two sets cannot be distinguished within typical *Hinode* noise.

- Sánchez Almeida, J. 2004, in Astronomical Society of the Pacific Conference Series, Vol. 325, The Solar-B Mission and the Forefront of Solar Physics, ed. T. Sakurai & T. Sekii, 115
 Sánchez Almeida, J. & Ichimoto, K. 2009, A&A, 508, 963
 Sánchez Almeida, J., Bonet, J. A., Viticchié, B., & Del Moro, D. 2010, ApJ, 715, L26
 Shimizu, T., Lites, B. W., Katsukawa, Y., et al. 2008, ApJ, 680, 1467
 Skumanich, A. & Lites, B. W. 1987, ApJ, 322, 473
 Socas-Navarro, H. & Sánchez Almeida, J. 2002, ApJ, 565, 1323
 Spruit, H. C. 1981, A&A, 102, 129
 Stenflo, J. O. 2009, Memorie della Societa Astronomica Italiana, 80, 690
 Tsuneta, S., Ichimoto, K., Katsukawa, Y., et al. 2008, Sol. Phys., 249, 167
 Vögler, A. & Schüssler, M. 2007, A&A, 465, L43
 Wedemeyer-Böhm, S. 2008, A&A, 487, 399
 Zhang, J., Yang, S.-H., & Jin, C.-L. 2009, Research in Astronomy and Astrophysics, 9, 921

Appendix A: Lack of crosstalk between magnetic field strength and magnetic field inclination

When Q and U are too small to be used, the inversions assume the magnetic field to be longitudinal. It is important to realize that such assumption does not influence our magnetic field strength diagnostics. When the polarizations signals are weak (our case), and the inclination is constant (our assumption), then Stokes V scales with the cosine of the inclination independently of the field strength (Sánchez Almeida & Trujillo Bueno 1999, § 3.1). The information on the field strength is coded in the shape of Stokes V , whereas the magnetic field inclination modifies the scaling. Such scaling is independently obtained by the inversion code disguised as stray-light, therefore the inferred magnetic field strength and inclination are uncoupled. All quiet Sun inversions assume the pixels to be partly covered by magnetic fields, and the corresponding filling factor is determined as a free parameter of the inversion (stray-light factor). An error on the magnetic field inclination affects the stray-light factor, but it does not influence the magnetic field determination. Figure A.1 illustrate the argument. It shows Stokes I and V synthesized in two atmospheres that differ in stray-light factor f_{sl} and cosine of inclination $\cos \theta$, but they have the same product $\cos \theta (1 - f_{sl})$. The two pairs of Stokes profiles are indistinguishable within the noise of *Hinode* observations.